



HAL
open science

Oscillations of a micro bubble under a free interface

Gautier Dussuyer, Dan Soto, Dominique Legendre

► **To cite this version:**

Gautier Dussuyer, Dan Soto, Dominique Legendre. Oscillations of a micro bubble under a free interface. 25e Congrès Français de Mécanique, Nantes, 29 août-2 septembre 2022, Aug 2022, Nantes, France. hal-04280098

HAL Id: hal-04280098

<https://hal.science/hal-04280098v1>

Submitted on 13 Nov 2023

HAL is a multi-disciplinary open access archive for the deposit and dissemination of scientific research documents, whether they are published or not. The documents may come from teaching and research institutions in France or abroad, or from public or private research centers.

L'archive ouverte pluridisciplinaire **HAL**, est destinée au dépôt et à la diffusion de documents scientifiques de niveau recherche, publiés ou non, émanant des établissements d'enseignement et de recherche français ou étrangers, des laboratoires publics ou privés.

Oscillations of a micro bubble under a free interface

G. DUSSUYER^{a,b,*}, D. SOTO^b, D. LEGENDRE^a

a. Institut de Mécanique des Fluides de Toulouse (IMFT), Université de Toulouse, CNRS, Toulouse, France.

b. Poietis, 27 Allée Charles Darwin 33600 Pessac

* Email : gautier.dussuyer@toulouse-inp.fr

Résumé :

Le but de ces travaux est d'étudier, grâce à la simulation numérique directe l'interaction entre une bulle et une surface libre. Une telle interaction a lieu lors du procédé LIFT (Laser-Induced Forward Transfer). Ce nouveau procédé d'impression sans contact consiste à focaliser un laser dans un milieu fluide afin de créer une bulle de cavitation qui va grossir et finalement éjecter le fluide qui l'entoure. Pour étudier ce problème, on considère une bulle sujette à une pression excessive (induite par l'input d'énergie laser) localisée à une distance contrôlée de la surface libre. En considérant des paramètres appropriés, deux jets verticaux (ascendant et descendant) sont générés après la forte expansion de la bulle. Un second jet ascendant plus large et plus lent est ensuite observé. L'objectif de ces travaux est de discuter des effets des paramètres principaux du problème sur les différentes phases du problème, et en particulier des conditions initiales imposées à la bulle ainsi que la distance de la bulle à l'interface. Afin de s'assurer de la validité du code utilisé, une première étape de validation des oscillations de la bulle en milieu infini est effectuée avant d'étudier l'effet de la présence de l'interface.

Abstract :

The aim of this work is to investigate, using direct numerical simulation, the interaction of a bubble (after its generation) with a free interface. Such interaction takes place in the LIFT (Laser-Induced Forward Transfer) process. This cutting edge printing technique is nozzle free. It consists of focusing a laser in a liquid so that a cavitation bubble is nucleated. This bubble will expand and finally ejects the surrounding liquid.

To study this problem, a bubble at a pressure P_0 located at a given distance of the interface is considered. When choosing appropriated parameters, two vertical jets (ascending and descending) are generated after the rapid bubble expansion. A secondary upward jet, thicker and slower is then observed. The aim of this work is to discuss the effect of the main parameters on the different phases of the process, and in particular the effects of the initial conditions as well as the initial distance between the bubble and the interface. In order to ensure that our code is accurate, a first validation step on bubble oscillations in an infinite media is done before investigating the interaction with the interface.

Mots clés : Bubble, free surface interaction, compressible, laser jet-induced, bio-printing.

Introduction

The aim of this work is to investigate, using direct numerical simulation, the interaction of a bubble (after its generation) with a free interface. Such interaction takes place in the LIFT (Laser-Induced Forward Transfer) process. This cutting edge printing technique is nozzle free. It consists of focusing a laser in a material so that a cavitation bubble is nucleated. This bubble will expand and finally ejects the surrounding material [1]. It is a very precise printing technique which has a lots of applications, including bio-printing and which has raised a certain interest in fundamental research from both experimental [2] and numerical sides [3]. Before studying the interaction between an oscillating bubble and an interface, a validation of our code is done for the case of an oscillating bubble in an infinite media where a theoretical solution is available (thanks to the Rayleigh Plesset equation). This equation takes into account viscosity and surface tension effects and makes the hypothesis of an incompressible liquid. For the cases with an interface, the induced jets are strongly linked to the first two oscillations of the bubble. Therefore we want our code to precisely describe at least the first two oscillations. It will be our criteria whether to know if our code is valid for the set of parameters chosen. Once the code is validated against the Rayleigh Plesset equation for the bubble oscillations in an infinite case, the oscillation close to an interface is considered with the objective to describe the bubble behaviour as well as the induced liquid jet formation. In order to understand better the role of each parameter in the physics involved, a parametric study is conducted.

1 Problem statement

The problem studied corresponds to the oscillations of a bubble of initial radius R_0 , first in a infinite media (Figure 1a) and then close to an interface (Figure 1b). The oscillations are produced thanks to an initial pressure P_0 at the initial time. For given fluid properties, Bubble oscillations are controlled by the couple (P_0, R_0) .

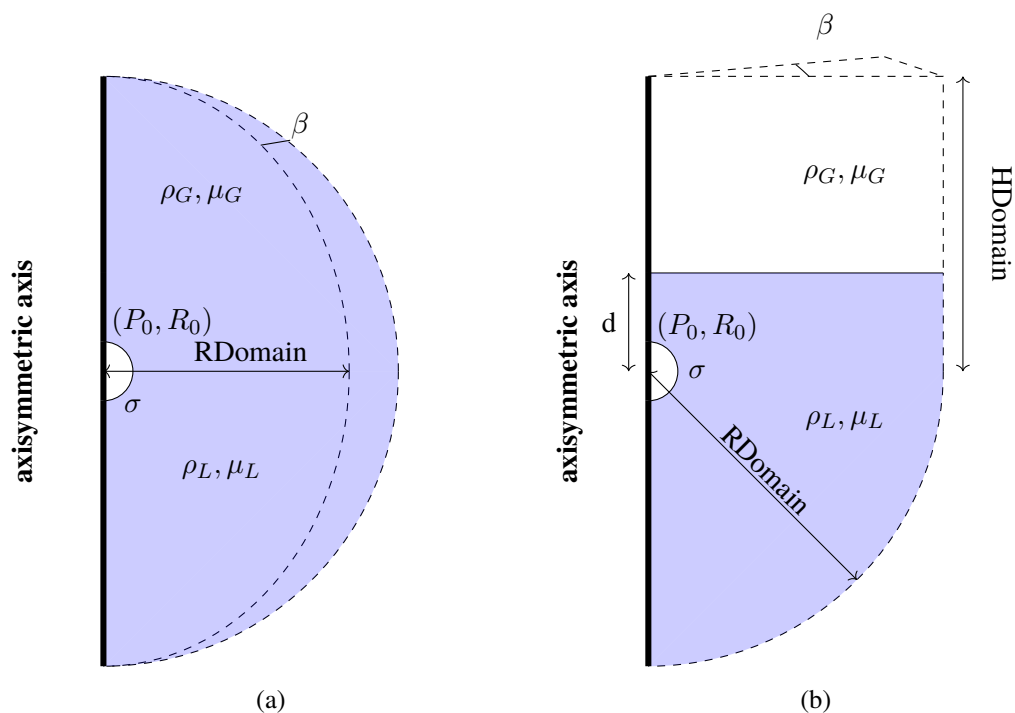


FIGURE 1 – CFD domain definition for (a) an infinite media and (b) with an interface

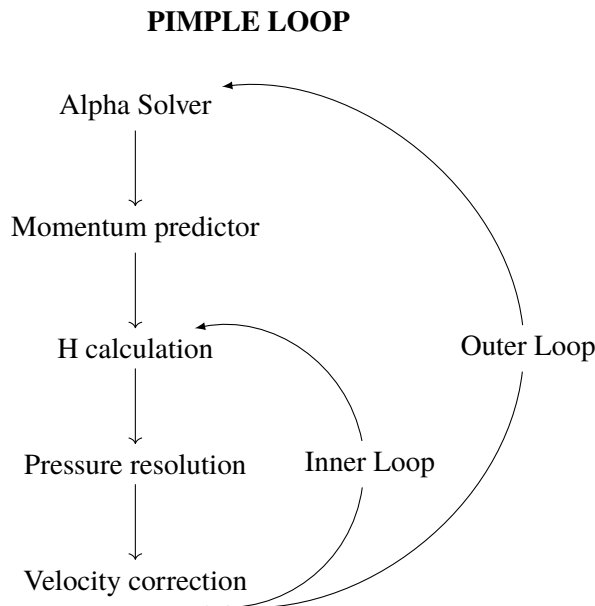


FIGURE 2 – Scheme of the PIMPLE algorithm (inside a time-step)

The other parameters correspond to the physical properties of the liquid and gas studied. All the parameters used in the reference case are precised in Table 1 :

| | | |
|--------------------|----------|----------------------|
| Initial conditions | P_0 | 5 bar |
| | R_0 | 100 μm |
| Liquid properties | ρ_L | 998.2 kg/m^3 |
| | μ_L | 20 <i>cPoise</i> |
| Gas properties | ρ_G | Perfect Gas |
| | μ_G | 0.0184 <i>cPoise</i> |
| Liquid / Gas | σ | 72.8 mN/m |

TABLE 1 – Parameter definitions and values considered in this study.

2 Presentation of the code

The code used for the study is based on the solver `compressibleInterFoam` from OpenFOAM [4]. `compressibleInterFoam` is a segregated compressible two phase flow CFD solver which uses a Volume of Fluid (VOF) method for the interface treatment. The details of the numerical implementation are given in the following. The link between each solver is schematized (Figure 2).

Several classes of VOF methods exist, with the main objective to control the interface shape and numerical thickness [5]. Among these methods, the compressive method is employed here. A "compressive term" is added in the VoF equation used to solve the the volume fraction α in order to maintain the sharpness of the interface.

$$\frac{\partial(\alpha)}{\partial t} + \nabla \cdot (\alpha v) + \nabla \cdot (\alpha(1 - \alpha)v_r) = \alpha(1 - \alpha) \left(\frac{1}{\rho_2} \frac{d\rho_2}{dt} - \frac{1}{\rho_1} \frac{d\rho_1}{dt} \right) + \alpha \nabla \cdot v \quad (1)$$

Boundedness of α is guaranteed by the MULES algorithm which is based on the method of flux corrected

transport where an additional limiter is used to cut-off the face-fluxes at critical values [6].

The surface tension term f_σ in the momentum equation is modelled with the continuum surface force method. Its effect is distributed across several cells. More informations on this method can be found on [7]. the interface curvature is evaluated using

$$K = \text{div}\left(\frac{\nabla C}{\|\nabla C\|}\right) \quad (2)$$

The fluid properties are then defined using the volume fraction α by :

$$\rho = \alpha\rho_1 + (1 - \alpha)\rho_2 \quad (3)$$

$$\mu = \alpha\mu_1 + (1 - \alpha)\mu_2 \quad (4)$$

Once discretized the momentum equation can be expressed as

$$MU = -\nabla P + f_\sigma \quad (5)$$

where P is the pressure and M a matrix that contains the discretization for the U terms in the momentum equation. Solving this equation is called the predictor step. At this stage continuity is not ensured. M is decomposed as a diagonal matrix A and a matrix H as followed :

$$MU = AU - H \quad (6)$$

A laplacian equation for the pressure needs to be solved to know its value.

$$\nabla \cdot (A^{-1}H) = \nabla \cdot (A^{-1}(-\nabla P + f_\sigma)) \quad (7)$$

Once the pressure is known, velocity is calculated thanks to

$$U = A^{-1}H - A^{-1}\nabla P - A^{-1}f_\sigma \quad (8)$$

The outer loop number in the PIMPLE algorithm is set to a relatively high number, typically 50. A criteria is imposed on the pressure solver so that the number of loop can be reduced if a convergence is reached. The inner loop is set to 3. Classical implicit Euler scheme is used for temporal discretization, combined with subcycles on the alpha solver.

Time step is limited by two Courant numbers :

- Co which is the classical Courant number, taking the whole domain into consideration
- αCo which is the Courant number taking into account only the domain close to the interface(s).

In our calculations, Co is limited by $Max(Co) = 0.5$ and αCo is limited by $Max(\alpha Co) = 0.2$.

Linear Upwind scheme is employed for convection term whereas second order centered scheme is used for diffusion term.

3 Validation against Rayleigh Plesset equation

The CFD code ability to consider bubble oscillation is first validated by considering bubble oscillations in an infinite media. The results are compared to the Rayleigh Plesset equation to quantify its precision and to check the influence of different parameters on the results.

3.1 Domain and Mesh

The domain is schematized in Figure 1a. It is a part of the 3D volume considering axisymmetric condition of the considered problem. An azimuthal angle $\beta = 5^\circ$ is considered. The domain radius is referred after as R_{Domain} . l_c corresponds to the distance around the bubble where the cell size is constant and is equals to δ_{min} . Cells size then gradually increases from δ_{min} to δ_{max} up to the domain boundary. All the domains and meshes characteristics are summed up in Table 2.

| | Reference Mesh | Fine Mesh | Coarse Mesh | Small Domain | Large Domain |
|--------------------------------|----------------|-------------|-------------|-------------------|--------------------|
| R_{Domain} | 10mm | 10mm | 10mm | 5mm | 20mm |
| l_c | 340 μm | 340 μm | 340 μm | 340 μm | 340 μm |
| Min cell size : δ_{min} | 2 μm | 1 μm | 4 μm | 2 μm | 2 μm |
| Max cell size : δ_{max} | 200 μm | 100 μm | 400 μm | $\sim 97.65\mu m$ | $\sim 405.59\mu m$ |
| Total number of cells | 308 898 | 1 235 592 | 76 832 | 256 328 | 364 658 |

TABLE 2 – Domains and meshes characteristics. The reference mesh is the mesh used in the study.

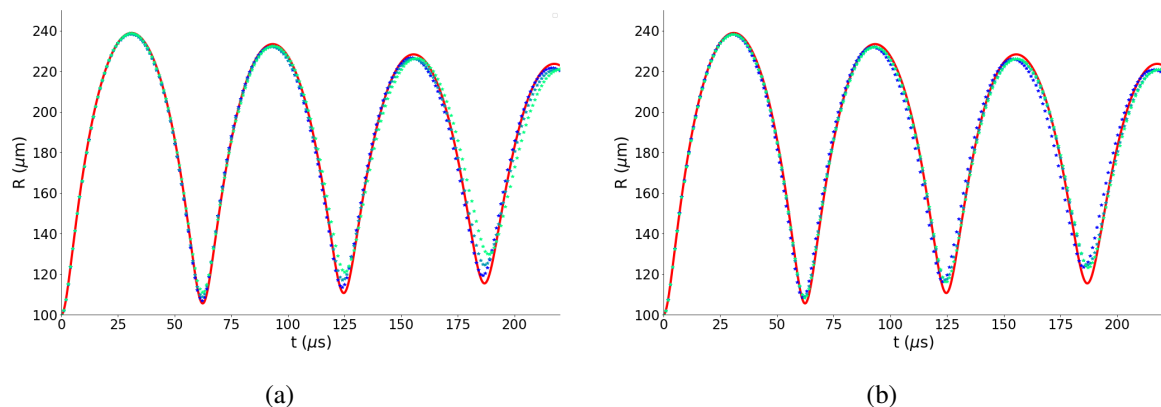


FIGURE 3 – Effect of the mesh resolution and the domain size. (a) Effect of the Meshes refinement. Theory (—), $\delta_{min} = 1\mu m$ (*), $\delta_{min} = 2\mu m$ (*), $\delta_{min} = 4\mu m$ (*). (b) Effect of the Domain size. Theory (—), $R_{Domain} = 5mm$ (*), $R_{Domain} = 10mm$ (*), $R_{Domain} = 20mm$ (*)

The simulations performed with the different meshes are reported in Fig. 3. The physical properties are given in Table 1. No significant differences are observed between the fine and the reference meshes during the first three oscillations. With the coarse mesh, the third rebound is much more damped than with the other meshes. With the three different domains, the same oscillations are obtained.

3.2 Bubble sphericity conservation

The evolution of the bubble sphericity is now checked, at least during the first two oscillations, which are the most important for the LIFT process, as it will be described in the next section. In Figure 4 the

bubble shape evolution is reported and compared to the exact spherical shape.

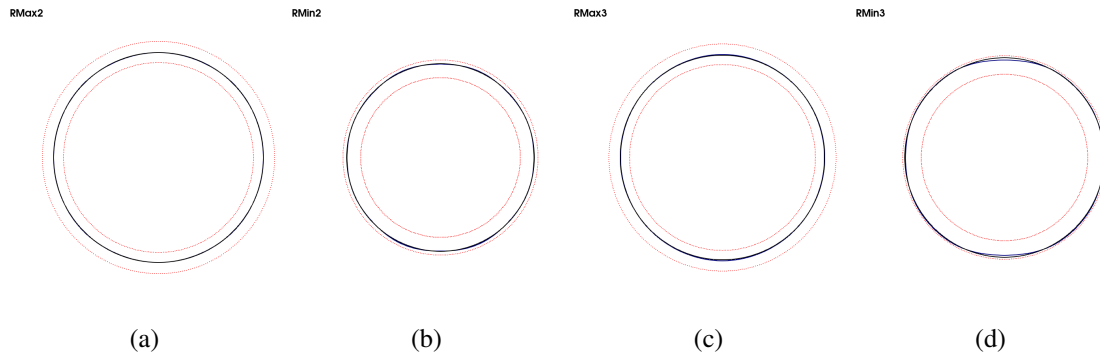


FIGURE 4 – Numerical Bubble shape (—) compared to the exact shape (—). The dotted red lines (--) indicate the theoretical bubble with a deviation of +5% and -5%, respectively. Second oscillation : (a) at the maximum radius and (b) and the minimum radius. Third oscillation : (c) at the maximum radius and (d) and the minimum radius

In the studied conditions, the bubble interface remains spherical during all the bubble oscillation and the difference between the bubble theoretical and simulated radius always stays in the interval $[-5\%; +5\%]$ (see Figure 4).

Numerical errors can be the source of non-physical interface deformations. In our oscillating system, they are particularly visible when the bubble radius is close to its minimum [8]. In particular, numerical errors in the discretization of the surface tension term coupled with the transport of the volume fraction result in the apparitions of spurious currents able to significantly deform and alter the interface shape. Viscosity tends to reduce spurious currents since their magnitude is known to evolve as σ/μ [9].

In Figure 5, the shape of the bubble observed for the first three rebounds are represented for different viscosities. As expected, the more the fluid is viscous, the more the bubble interface remains spherical. At the end of the first oscillation (Figure 5a), the bubble is spherical for all the considered viscosities. However at the end of the second oscillation (Figure 5b), the bubble interface is considerably deformed for the fluid with the smaller viscosity of $\mu = 1cPoise$. At the end of the third oscillation (Figure 5c), bubble interface is completely deformed for the fluid with viscosity of $\mu = 1cPoise$ and it has been fragmented. The interface is slightly deformed for fluids with $\mu = 5cPoise$ and $\mu = 10cPoise$. For viscosities of $20cPoise$ and more, the interface is perfectly spherical.

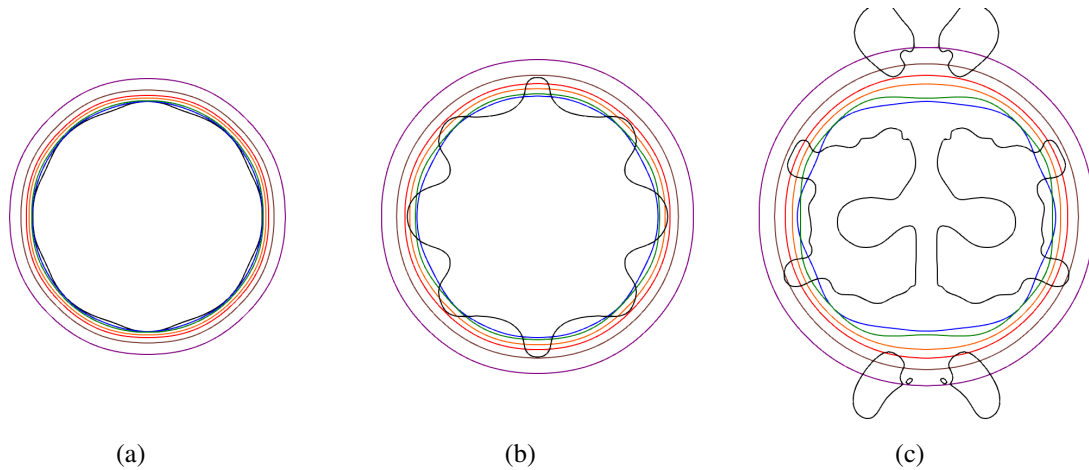


FIGURE 5 – Influence of viscosity on bubble shape. $\mu = 1cPoise(-)$, $\mu = 5cPoise(-)$, $\mu = 10cPoise(-)$, $\mu = 20cPoise(-)$, $\mu = 30cPoise(-)$, $\mu = 50cPoise(-)$, $\mu = 100cPoise(-)$. (a) first oscillation, (b) second oscillation and (c) third oscillation.

3.3 Summary on the code performance

With the considered parameters, the CFD code used for our study can accurately describe the two first bubble oscillations in a infinite media. The simulation results robustness has been validated thanks to a domain and mesh sensibility study. The three considered domains give the same bubble oscillations and very few difference between the fine and the reference mesh are observed on the two first bubble oscillations. The limits of the code have been observed when changing the liquid viscosity. A special attention must be paid on this parameter. Indeed the code performance is clearly reduced when decreasing the viscosity due to the development of the well identified spurious currents.

4 Bubble oscillations near an interface

4.1 Description of the process

The domain used for the simulations is reported in Figure 1b. The reference cell size chosen (near the bubble) is $2\mu m$ (i.e the same as the previous part). The domain radius R_{Domain} is $5mm$ and its height H_{Domain} is $2mm$.

Figure 6 reports some typical bubble shape during its oscillation and interaction with the interface. A bubble of radius $R_0 = 100\mu m$ is initially located at the distance $d = 150\mu m$ under the interface. During the initial stages of the process, the bubble expands and deforms the interface. Due to the presence of the interface, the bubble expansion is no longer the same in each direction (see Figure 6a). Indeed the mass of liquid to displace above the bubble is lower, therefore the upper direction is the preferred for the bubble expansion. Once the bubble has reached its maximum expansion, two jets are generated : one jet directed upwards and one counter-jet directed towards the bubble (see Figure 6b). This counter-jet will then pierces the bubble. The jet is then followed by a wider jet, here called secondary jet (see Figure 6c).

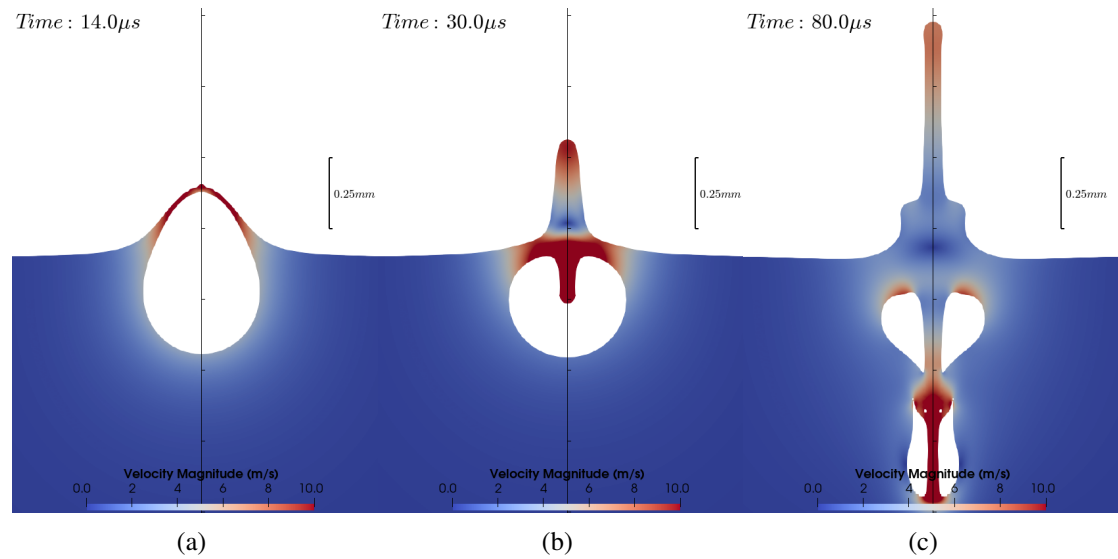


FIGURE 6 – Near-interface bubble oscillations characteristics steps for $R_0 = 100\mu\text{m}$ and $d = 150\mu\text{m}$: (a) Bubble expansion, (b) Jet and counter jet and (c) Secondary jet.

Figure 7 compares the time evolution of the bubble equivalent radius with and without the presence of the interface. As it can be seen in Figure 7, the oscillatory system is more damped with the interface.

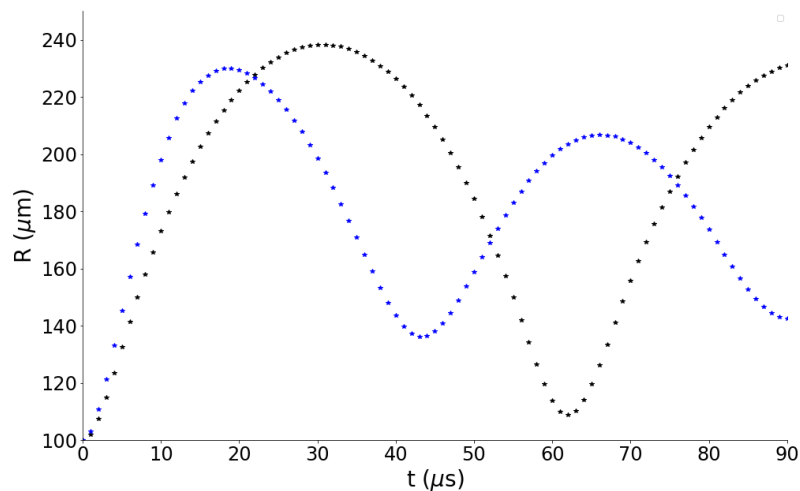


FIGURE 7 – Bubble radius along time in an infinite media (\star) and near an interface (\star).

4.2 Liquid ejection

As described, the counter-jet then pierces the bubble and a secondary jet, thicker is created (see Figure 8a). For the LIFT process, the aim is to transfer some liquid on a receiver located at a certain distance above the interface. To do so, the liquid must reach a certain height. Therefore we propose to post process the volume above a certain height for different cases. The height chosen is $350\mu\text{m}$ above the interface and the bubble initial radius is $R_0 = 100\mu\text{m}$. In Figure 8a), the time evolution of the liquid displaced above the distance to the interface $Z = 350\mu\text{m}$ is plotted. The figure clearly show a change of slope at

$t \sim 125 \mu s$. The first part ($t \in [25, 125] \mu s$) is the volume transported by the first jet while the second part ($t \geq 125 \mu s$) is the volume transported by the second jet. The volume transported by this jet is much more important than the one transported by the first jet (see the slope breaking Figure 8b at $t \sim 125 \mu s$).

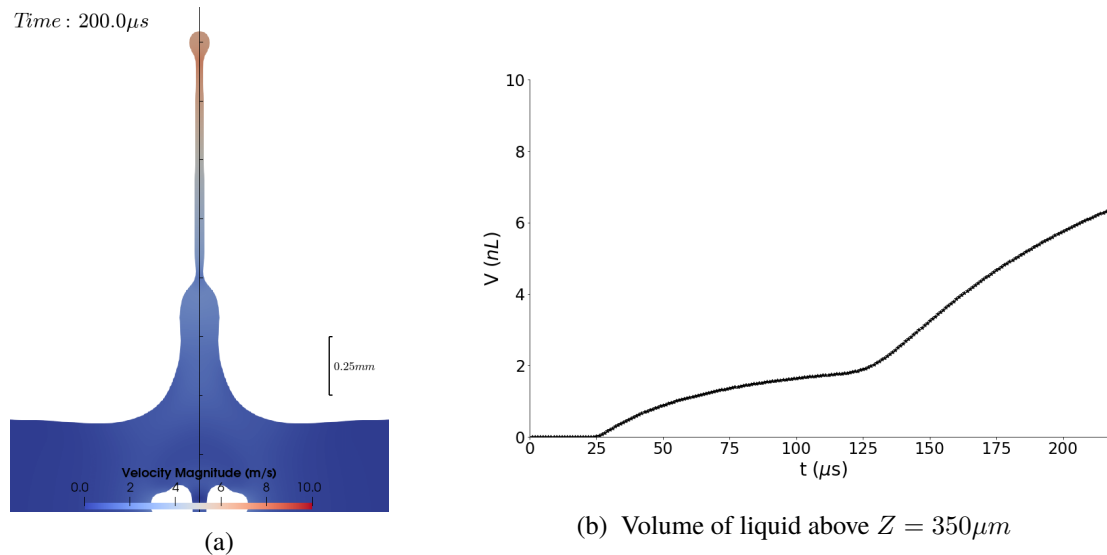


FIGURE 8 – (a) Secondary jet shape and (b) plot of the volume of liquid above $Z = 350 \mu m$ along time

4.2.1 Effect of the bubble distance to the interface

In order to understand better the interaction between the bubble and the interface, a parametric study is now presented by varying the normalized distance $H^* = d/R_0$. Figure 9 reports the bubble evolution at three different time for the five different values of H^* considered. A clear impact of H^* is observed on the jets formation. The closer the bubble is to the interface, the more the bubble deforms during its expansion (see Figure 9a). The quantification of the deviation from the spherical shape has been evaluated with maximum bubble aspect ratio. It is reported in Figure 10a for different values of H^* . The bubble is clearly more deformed when H^* is reduced. When the bubble is close to the interface, the jet and counter jet are more developed as shown in Figure 9b. For the case where $H^* = 5$, the counter jet has not been able to pierce the bubble (see Figure 9c). The time evolution of the liquid jet is reported in Figure 10b for the considered values of H^* . The figure confirms that no jet is created for $H^* > 3$.

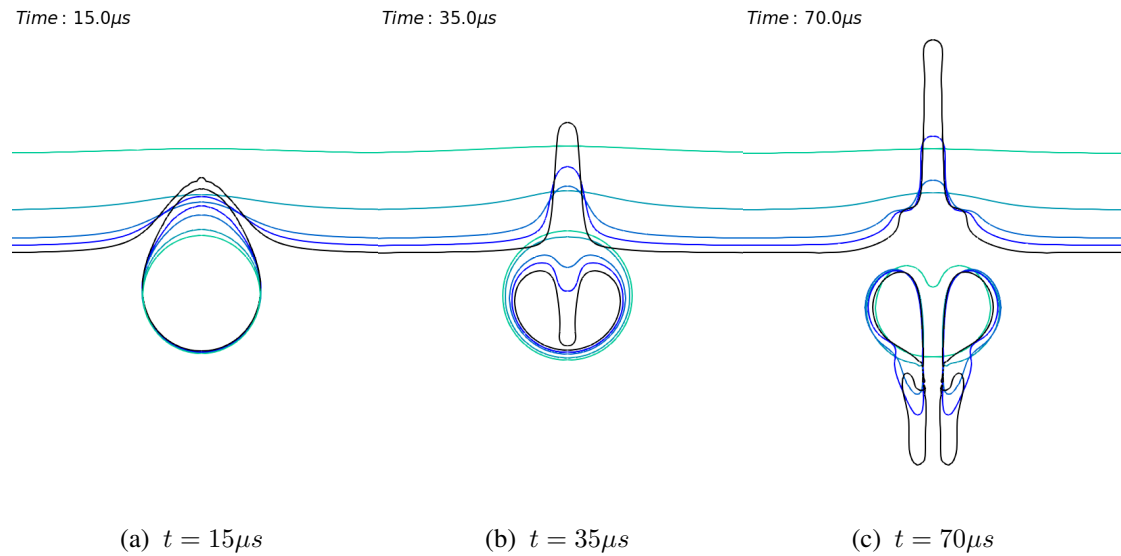


FIGURE 9 – $H^* = 1.5$ (—); $H^* = 1.75$ (—); $H^* = 2$ (—); $H^* = 3$ (—); $H^* = 5$ (—) at different times

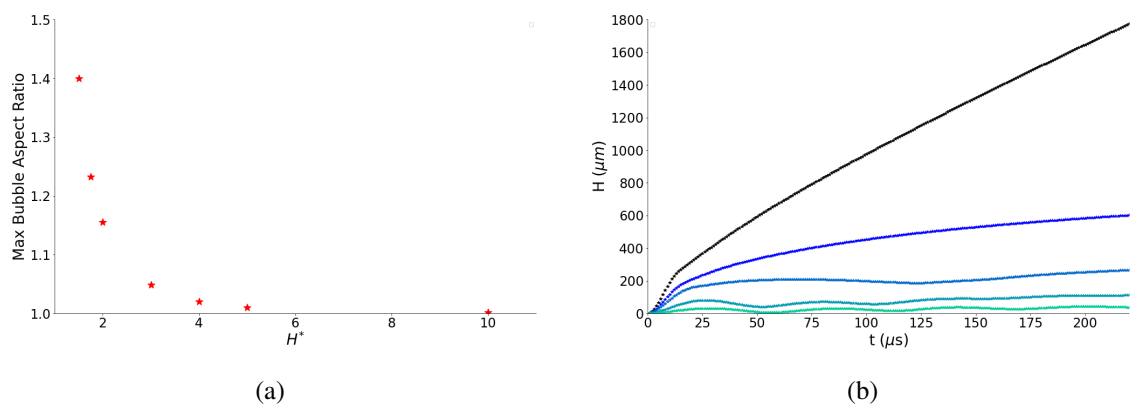


FIGURE 10 – Effect of the distance to the interface on bubble oscillation. (a) Bubble maximum aspect ratio as a function of H^* . (b) Jet height time evolution for $H^* = 1.5$ (★); $H^* = 1.75$ (★); $H^* = 2$ (★); $H^* = 3$ (★); $H^* = 5$ (★).

4.2.2 Effect of the initial conditions R_0 and P_0

As shown in the previous section, there is no liquid transfer for $H^* = 2$, $H^* = 3$ and $H^* = 5$. This is confirmed by Figure 11a where the volume of liquid transferred at the distance $Z = 350\mu m$ is reported as a function of time. For $H^* = 1.75$, the transfer is possible but the volume transferred is small. However, for $H^* = 1.5$, an important volume of liquid can be transferred.

Figure 11b reports the effect of the initial pressure P_0 on the volume of liquid transferred at the distance $Z = 350\mu m$. For $P_0 = 5bar$ and $P_0 = 6bar$ important volumes of liquid can be transferred. The transfer of small volumes is still possible for $P_0 = 4bar$ but no transfer is observed for $P_0 = 3bar$.

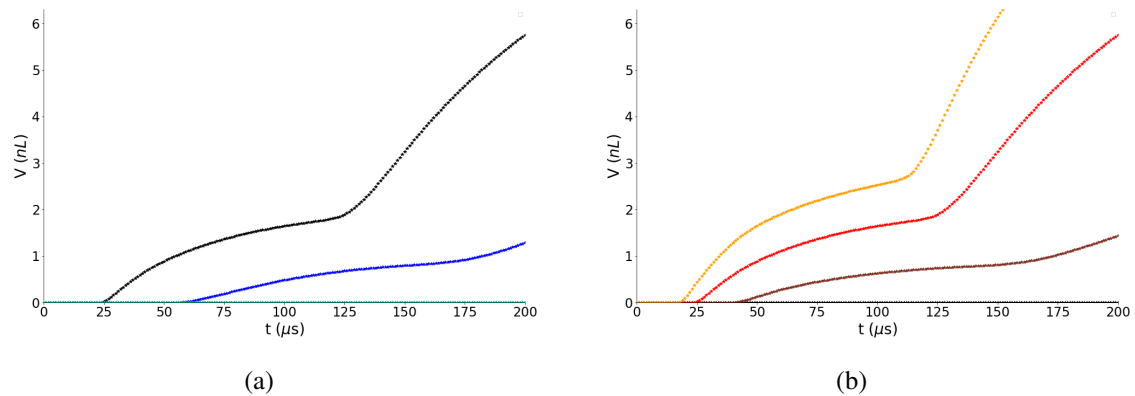


FIGURE 11 – Volume of liquid at $Z > 350 \mu\text{m}$ above the interface as a function of time. (a) effect of the bubble to interface distance H^* : $H^* = 1.5$ (*); $H^* = 1.75$ (*); $H^* = 2$ (*); $H^* = 3$ (*); $H^* = 5$ (*). (b) Effect of the initial pressure P_0 : $P_0 = 3\text{bar}$ (*); $P_0 = 4\text{bar}$ (*); $P_0 = 5\text{bar}$ (*); $P_0 = 6\text{bar}$ (*)

5 Conclusion

Our CFD code has been validated against the Rayleigh Plesset equation for bubble oscillations in an infinite media. In particular, the viscosity effects on the solver accuracy has been shown. Around 1cPoise, our solver is not able to model accurately two bubble oscillations in a infinite media.

The near-interface bubble oscillations process has been detailed : three main phases have been identified :

- the bubble expansion phase
- the generation of a an upward jet and a counter jet (directed downward)
- the generation of a thicker but slower second jet

The effect of the initial bubble pressure and the bubble-interface distance have been reported. The more the bubble is close to the interface, the more it is deformed with a direct influence on the jet development. Increasing the pressure parameter also increase bubble deformation and the jet development. By post-processing volume of liquid which reach a certain height, three regimes have been identified.

- No transfer regime : the liquid is not ejected height enough. A receiver located at the height chosen will not received any liquid.
- Small volume transfer regime : the liquid reaches the virtual receiver height but the secondary jet volume slop is not very steep therefore the volume that can be transferred is small.
- Large Volume transfer regime : The volume carried by the second jet is much more important than the one carried by the first one. Large volume can be transferred.

Remerciements

This work was granted access to the HPC resources of CALMIP supercomputing center under the allocation 2020-P1519.

Références

- [1] P. SERRA et A. PIQUÉ, *Laser-Induced Forward Transfer : Fundamentals and Applications*, 2019. adresse : <https://onlinelibrary.wiley.com/doi/epdf/10.1002/admt.201800099>.
- [2] R. T. CERBUS, H. CHRAIBI, M. TONDUSSON, S. PETIT, D. SOTO, R. DEVILLARD, J. P. DELVILLE et H. KELLAY, *Experimental and numerical study of laser-induced secondary jetting*, 2022. adresse : <https://doi.org/10.1017/jfm.2021.1117>.
- [3] Y. SAADE, M. JALAAL, A. PROSPERETTI et D. LOHSE, *Crown formation from a cavitating bubble close to a free surface*, 2021. adresse : <https://doi.org/10.1017/jfm.2021.676>.
- [4] OPENFOAM, <https://www.openfoam.com>. adresse : <https://www.openfoam.com/>.
- [5] V. R. GOPALA et B. G. M. VAN WACHEM, *Volume of fluid methods for immiscible-fluid and free-surface flows*, 2008. adresse : <https://doi.org/10.1016/j.cej.2007.12.035>.
- [6] S. T. ZALESAK, *Fully multidimensional flux-corrected transport algorithms for fluids*, 1978. adresse : [https://doi.org/10.1016/0021-9991\(79\)90051-2](https://doi.org/10.1016/0021-9991(79)90051-2).
- [7] J. U. BRACKBILL, D. B. KOTHE et C. ZEMACH, *A continuum method for modeling surface tension*, 1992. adresse : <https://www.sciencedirect.com/science/article/pii/S002199919290240Y>.
- [8] M. KOCH, C. LECHNER, F. REUTER, K. KÖHLER, R. METTIN et W. LAUTERBORN, *Numerical modeling of laser generated cavitation bubbles with the finite volume and volume of fluid method, using OpenFOAM*, 2015. adresse : <https://doi.org/10.1016/j.compfluid.2015.11.008>.
- [9] T. ABADIE, J. AUBIN et D. LEGENDRE, *On the combined effects of surface tension force calculation and interface advection on spurious currents within Volume of Fluid and Level Set frameworks*, 2015. adresse : <https://www.sciencedirect.com/science/article/pii/S0021999115003113>.